Infectious Disease Modelling 8 (2023) 253–269

Contents lists available at ScienceDirect

Infectious Disease Modelling

journal homepage: www.keaipublishing.com/idm

Assessing the spatiotemporal malaria transmission intensity with heterogeneous risk factors: A modeling study in Cambodia

Mutong Liu [a, b], Yang Liu [a, b, *], Ly Po [c], Shang Xia [b, d, e, f], Rekol Huy [c], Xiao-Nong Zhou [b, d, e, f], Jiming Liu [a, b, **]

[a] Department of Computer Science, Hong Kong Baptist University, Hong Kong Special administrative region of China
[b] HKBU-CSD & NIPD Joint Research Laboratory for Intelligent Disease Surveillance and Control, China
[c] National Center for Parasitology, Entomology & Malaria Control (CNM), Ministry of Health, Phnom Penh, Cambodia
[d] National Institute of Parasitic Diseases, Chinese Center for Disease Control and Prevention, Shanghai, China
[e] Key Laboratory of Parasite and Vector Biology, National Health and Commission of the People's Republic of China, Shanghai, China
[f] WHO Collaborating Center for Tropical Diseases, Shanghai, China

ARTICLE INFO

Article history:
Received 26 September 2022
Received in revised form 8 January 2023
Accepted 29 January 2023
Available online 1 February 2023
Handling Editor: Dr Yijun Lou

Keywords:
Malaria
Transmission intensity assessment
Spatiotemporal network
Computational approach
Heterogeneous risk factors

ABSTRACT

Malaria control can significantly benefit from a holistic and precise way of quantitatively measuring the transmission intensity, which needs to incorporate spatiotemporally varying risk factors. In this study, we conduct a systematic investigation to characterize malaria transmission intensity by taking a spatiotemporal network perspective, where nodes capture the local transmission intensities resulting from dominant vector species, the population density, and land cover, and edges describe the cross-region human mobility patterns. The inferred network enables us to accurately assess the transmission intensity over time and space from available empirical observations. Our study focuses on malaria-severe districts in Cambodia. The malaria transmission intensities determined using our transmission network reveal both qualitatively and quantitatively their seasonal and geographical characteristics: the risks increase in the rainy season and decrease in the dry season; remote and sparsely populated areas generally show higher transmission intensities than other areas. Our findings suggest that: the human mobility (e.g., in planting/harvest seasons), environment (e.g., temperature), and contact risk (coexistences of human and vector occurrence) contribute to malaria transmission in spatiotemporally varying degrees; quantitative relationships between these influential factors and the resulting malaria transmission risk can inform evidence-based tailor-made responses at the right locations and times.

* Corresponding author. Department of Computer Science, Hong Kong Baptist University, Hong Kong Special administrative region of China.
** Corresponding author. Department of Computer Science, Hong Kong Baptist University, Hong Kong Special administrative region of China.
E-mail addresses: csygliu@comp.hkbu.edu.hk (Y. Liu), jiming@comp.hkbu.edu.hk (J. Liu).
Peer review under responsibility of KeAi Communications Co., Ltd.

https://doi.org/10.1016/j.idm.2023.01.006

1. Introduction

Malaria is one of the oldest yet life-threatening infectious diseases. The World Health Organization (WHO) reported in 2021 that malaria places nearly four billion people at risk and creates heavy public health burdens in over 80 countries, especially low-income and undeveloped countries (World Health Organization, 2021b). Moreover, the emergence and exacerbation of artemisinin resistance in parasites and resistance of mosquitoes to insecticides, which could reverse all efforts to control and prevent malaria and lead to large-scale outbreaks and epidemics, necessitate the acceleration of malaria elimination (Phyo & Nosten, 2018; World Health Organization, 2021a).

To effectively control and eliminate malaria, a comprehensive and accurate assessment of the malaria transmission intensity is essential, as it can inform public health policies and decisions pertaining to the deployment of tailor-made intervention strategies (Battle et al., 2019; Routledge et al., 2018; Weiss et al., 2019; World Health Organization, 2017). However, it is difficult to accurately assess this intensity because it is spatiotemporally varying and influenced by heterogeneous risk factors originating from vectors, humans, and the environment. For example, vector species and their population densities vary in space and time due to their different preferences for survival conditions and habitats (Obsomer et al., 2013), resulting in an uneven distribution of the malaria transmission intensity (Moyes et al., 2016; Suwonkerd et al., 2013). Furthermore, human mobility, mainly driven by socioeconomic factors, leads to the risk of importing malaria from epidemic areas and re-establishes outbreaks in malaria-free areas (Grietens et al., 2015; Guyant et al., 2015; World Health Organization & Regional Office for South-East Asia, 2017). The environmental conditions in an area, such as temperature, rainfall, and land cover, also greatly influence the malaria transmission potential by directly or indirectly impacting the biological features of mosquitoes and parasites (Ceccato et al., 2012; Eikenberry & Gumel, 2018; Munga et al., 2006, 2009; Stefani et al., 2013) as well as human activities (Kerkhof et al., 2016). These risk factors influence each other, making the precise measurement of the malaria transmission intensity challenging.

To provide scientifically grounded guidance for effective malaria control, we need to answer a critical question: How can we accurately assess the spatiotemporal malaria transmission intensity by comprehensively incorporating heterogeneous risk-related factors for mapping custom-designed intervention strategies at different locations and time periods? Some popular indicators have already been developed to assess the intensity or risk of malaria transmission based on domain knowledge. As a standard indicator, annual parasite incidence (API), which denotes the number of confirmed malaria cases in a specific year, is officially used by the WHO malaria elimination framework to classify malaria transmission intensity for strategizing national malaria elimination plans (World Health Organization, 2017). Although the API can describe the malaria risk based on available observational malaria cases, the variability of intensity (e.g., seasonal differences) is not well captured; and it cannot indicate the future trends of the epidemic (e.g., persistence, outbreak, or die-out) under different transmission and intervention conditions (Cohen et al., 2017). To provide more information of disease propagation, other theoretical metrics have been introduced to quantify the malaria transmission intensity with respect to different risk-related factors from two perspectives: the local transmission risk (i.e., inherent potential for transmitting malaria) and the imported risk (World Health Organization, 2017). For local transmission risk, the vectorial capacity (VCAP, i.e., the expected number of infectious bites from mosquitoes per day brought by a single infectious case), the entomological inoculation rate (EIR, i.e., the expected number of infectious bites from mosquitoes per day per human), and the basic reproduction number (R_0, i.e., the expected number of infected cases which is brought by a single infectious case) are widely adopted to evaluate the transmission potential and guide intervention planning (Brady et al., 2016; Routledge et al., 2018; Smith & McKenzie, 2004). However, these metrics do not fully consider the heterogeneity of vectors and environments (Ceccato et al., 2012; Shi et al., 2020), such as the distributions of the dominant vector species and different types of land covers (Munga et al., 2006, 2009; Mushinzimana et al., 2006). When measuring imported risks, there has been a focus on identifying the characteristics of mobile and migrant populations (MMPs) and assessing the risk level of MMPs (Grietens et al., 2015; World Health Organization & Regional Office for South-East Asia, 2017). However, such risk level does not quantitatively consider spatiotemporal variations in human mobility and thus could only provide qualitative information for the transmission intensity at an approximate level, which is insufficient for accurate and timely policymaking.

In addition to the aforementioned indicators and metrics of malaria transmission intensity, many studies have assessed the transmission intensity and predicted malaria risk from a computational modeling perspective. Existing work of computational modeling could be divided into two categories: mechanism-based models and data-driven models. Mechanism-based models, also known as compartmental models, are designed based on the understanding of malaria transmission mechanisms (Chitnis et al., 2010; Mandal et al., 2011). They usually depict the biological transmission process between humans and vectors by a set of ordinary differential equations or difference equations, such as the most classical Ross-Macdonald model (Macdonald, 1957) and its variants that further consider other transmission-related characteristics, e.g., the human immunity level (Yang, 2000), non-linear forces of infection between humans and vectors (Olaniyi & Obabiyi, 2013), etc. In addition to the sophisticated compartmental models that describe the temporal dynamics of the whole population, many variants of the traditional compartmental models further incorporate transmission heterogeneity into the disease modeling. For instance, spatial heterogeneity can be introduced by modeling human and vector mobility (Cosner et al., 2009; Gao & Ruan, 2014; Prosper et al., 2012; Ruktanonchai et al., 2016); the heterogeneity of acquired immunity level can be reflected by the age structure (Filipe et al., 2007). The mechanism-based models can predict epidemic trends by simulation with the interpretable model structures and parameters with ideal assumptions. However, these models unavoidably simplify the real processes of infectious disease transmission; moreover, due to the predefined mechanisms, they are less flexible in incorporating other risk-related information when the domain knowledge is lacking. As a result,

mechanism-based models are limited in fully utilizing the risk-related observations for accurate predictions of disease transmission risks in real-world scenarios.

For data-driven models, we further divide them into two categories. The first category is classical statistical models. In this category, a wealth of studies focus on investigating the statistical relationships between the malaria risk (e.g., parasite prevalence, API, and EIR) and the available observations, which are generally the survey data collected from the field studies (e.g., malariometric surveys, cross-sectional studies, longitudinal studies, or entomological monitoring) (Cano et al., 2004; Kamya et al., 2015; Munga et al., 2009; Onori, 1967), and then mapping the risk in areas without the available survey data. Representative statistical models include discriminant analysis (Omumbo et al., 2002, 2005), multinomial regression model (G. J. Yang et al., 2010), multiple logistic regression (De Oliveira et al., 2013), Bayesian geostatistical models (Amoah et al., 2021; Bennett et al., 2013; Gemperli et al., 2006; Gething et al., 2012), and geostatistical zero inflated binomial and negative binomial models (Amek et al., 2012; Rumisha et al., 2014). These works usually provide malaria risk maps with high spatial resolution and low temporal resolution for understanding the malaria situation in a certain area and period. However, these models rarely consider the factor of human mobility across different locations during different seasons, which is of great importance in assessing the spatiotemporal malaria transmission intensity. The second category of data-driven models is representative machine learning (including state-of-the-art deep learning) models, which treat malaria risk prediction as a time-series prediction problem. These models generally predict the future disease dynamics of specific regions by modeling the spatiotemporal patterns of malaria transmission (local and imported) using historical case data and/or risk-related data. Many models in this category, however, are not designed for specific diseases and thus do not fully integrate disease-specific domain knowledge (Pei et al., 2018, 2022; Tan et al., 2021; Wu et al., 2018; Zhang et al., 2015). As a result, the impact of various risk-related factors on the disease transmission intensity or risk cannot be quantified in a precise way; and it is hard to provide clear guidance for decision-makers to implement time/location/factor-specific measures in response to potential risks or outbreaks according to the modeling results. Recent studies have started to incorporate some domain knowledge, such as the ordinary differential equations (Kargas et al., 2021; Wang et al., 2021) or the metrics (e.g., the VCAP and EIR) (Shi et al., 2017, 2020; B. Yang et al., 2014) that characterize the disease transmission process, into the data-driven models. However, many important vectorial and environmental factors impacting malaria transmission, such as the dominant vector species and the distribution of different land cover types, are not well incorporated into the existing data-driven models.

To address the above challenges, we present a computational model for accurately assessing the malaria transmission intensity and its spatiotemporal variations by representing the seasonal and geographical heterogeneities of vectorial, human, and environmental factors via a spatiotemporal transmission network. To validate the effectiveness of the proposed model, we conduct a case study on 15 malaria-severe districts in Cambodia, one of the most malaria-endemic countries in the Western Pacific Region (World Health Organization, 2021b). Although the number of malaria cases decreases greatly in recent decades in Cambodia (Ministry of Health Kingdom of Cambodia, 2021), i.e., the number of indigenous cases decreases from around 107,000 in 2001 to around 10,000 in 2020, the artemisinin resistance (Phyo & Nosten, 2018), the suitable climate and environment for mosquito breeding (Kar et al., 2014; Kerkhof et al., 2016; Suwonkerd et al., 2013), the hard-to-trace imported cases (Guyant et al., 2015), and the limited surveillance resources (Ministry of Health Kingdom of Cambodia, 2021) make malaria elimination in this region very challenging and necessitate better targeted control of malaria risk.

The case study demonstrates the effectiveness of the proposed model in terms of the accuracy of risk assessment and hotspot identification. More importantly, our quantitative and qualitative analyses of the time-varying transmission patterns among various districts show the potential of our model for identifying and stratifying local and cross-location malaria transmission risks attributed to various underlying factors, thereby providing quantifiable evidence to guide the development of tailor-made responses at targeted locations and times.

2. Material and methods

We present a model to assess the spatiotemporal malaria transmission intensity by constructing a dynamic malaria transmission network. The transmission network consists of two parts: the local intensity at each node (e.g., at each location) and the cross-location transmission intensity in the network. First, we introduce data sources and data preprocessing methods. Then, we present the representation of the vector density, which integrates human density, vector species, and land cover distributions, to provide a comprehensive characterization of the heterogeneity of local malaria transmission. Thereafter, we mathematically formulate the local malaria transmission process at each location and further extend the formulation to the situation of cross-location malaria transmission by incorporating a human mobility network. Finally, we integrate the local transmission intensity and the cross-location transmission intensity through a next-generation matrix and obtain the desired transmission network.

2.1. Data collection and preprocessing

We use the data from 15 districts with high risks of malaria transmission in recent years from six malaria-endemic provinces in Cambodia for our study. Specifically, the districts in our study are all located in six provinces with high burdens of malaria in the recent decade (Chhim et al., 2021), including two eastern provinces (Mondul Kiri and Ratanakiri), two northeastern provinces (Kratie and Stung Treng), and two western provinces (Pursat and Kampong Speu). Information on these districts is provided in Supplementary Table S1. We collected data in six categories: epidemiological data, climate data, geographical data, entomological data, demographic data, and socioeconomic data. For the epidemiological data, we used the monthly malaria

case number data from January 2018 to March 2021, collected by the community, i.e., the village malaria workers, in 15 aforementioned districts of Cambodia. The data were provided by the Cambodia National Center for Parasitology Entomology and Malaria Control (CNM). For the climate data, we used temperature and rainfall to calculate several parameters in the SLIS model that are time varying. We obtain gridded temperature data (Fan & van den Dool, 2008) with a spatial resolution of 0.5° latitude and 0.5° longitude and a monthly temporal resolution from the Physical Sciences Laboratory (PSL) website (GHCN CAMS: https://psl.noaa.gov/data/gridded/data.ghcncams.html, September 3, 2022, date last accessed). We also collected gridded rainfall data (Schneider et al., 2011) with a spatial resolution of 1.0° latitude and 1.0° longitude and a monthly temporal resolution from the PSL website (GPCC: https://psl.noaa.gov/data/gridded/data.gpcc.html, September 3, 2022, date last accessed). For the temperature and rainfall, we calculated the weighted average value of each district in each month using the inverse distance weighting (IDW) method instead of using the grid data directly. The reason is that the spatial resolution of temperature and rainfall data is too coarse to be adopted at the district level. The time range of the collected temperature and rainfall data was from November 2017 to March 2021, and we used a three-month average of collected data to avoid possible noise (Tanser et al., 2003). For example, we used the average of the temperature data in November 2017, December 2017, and January 2018 as the input value for January 2018. For the geographic data, we collected yearly land cover type data (Friedl & Sulla-Menashe, 2015) with a spatial resolution of 500 m × 500 m from the NASA Earth Science Data website (MCD12Q1: https://ladsweb.modaps.eosdis.nasa.gov/missions-and-measurements/products/MCD12Q1/, September 3, 2022, date last accessed). As the changes in land cover distribution over time were relatively small, we used the data from 2018 for all three years. Similar to the land cover data, we used the same latitude and longitude coordinates to obtain the corresponding vector distribution data (Moyes et al., 2016) from the website of the Malaria Atlas Project (https://malariaatlas.org/explorer/#/, September 3, 2022, date last accessed). We considered the *An. Dirus* complex and the *An. Minimus* complex in our study, which are two dominant types of vectors in Cambodia (Suwonkerd et al., 2013). We collected economic data at the district level in Cambodia from the website of the Statistics Bureau of Japan (http://www.stat.go.jp/english/info/meetings/cambodia/e11f_dc2.html, September 3, 2022, date last accessed). We used the number of persons engaged in establishments to represent the level of job opportunity in different districts. For the demographic data, we collected the human population density data for 2020 in Cambodia from the website of the Humanitarian Data Exchange (HDX) (https://data.humdata.org/dataset/cambodia-high-resolution-population-density-maps-demographic-estimates, September 3, 2022, date last accessed) (Facebook Connectivity Lab and Center for International Earth Science Information Network, 2016).

2.2. Formulation of vector density

Vector density has been used to evaluate the malaria transmission intensity from the perspective of mosquito abundance. As one type of entomological data, vector density is usually collected via field observations (Amek et al., 2012), providing finite sampling data that cover a small range over space and time. However, in some areas, there is a paucity of entomological data. Therefore, many studies have explored the quantitative relationship between the vector density and its related factors that are easily accessible (e.g., climate data), so as to estimate the vector density using these available data (Amek et al., 2012; Li et al., 2019; Rumisha et al., 2014).

Here, we introduce a comprehensive representation of vector density for a location (e.g., a district in our study) by combining the human and vector distributions for different types of land cover to explore the spatial heterogeneity of the vector density for measuring the local malaria transmission risk in an accurate way. Based on the assumed linear relationship between the mosquito population and rainfall (Ceccato et al., 2012; Connor, 2002; Shi et al., 2020), we integrate the mosquito density, which is based on the volume of rainfall, into a weighted linear function in terms of different types of land cover. Moreover, for each type of land cover, the estimation of vector density can be obtained based on the distribution of vector occurrence and that of the human population density for the selected type of land cover in a gridwise manner. Specifically, our formulation of vector density is given as follows:

$$\begin{aligned} m &= \frac{vector\ population}{human\ population} = \frac{pop_2}{pop_1} \\ &= \sum_{k=1}^{l} w_k \left(\frac{pop_{2,k}}{pop_{1,k}}\right) + m_0 \\ &= \sum_{k=1}^{l} \frac{G_{total}^k}{G_{total}} \left(\frac{1}{G_{total}^k} \sum_{g=1}^{G_{total}^k} \frac{pop_{2,k,g}}{pop_{1,k,g}}\right) + m_0 \\ &= \frac{1}{G_{total}} \sum_{k=1}^{l} \left(\sum_{g=1}^{G_{total}^k} \frac{o_{2,k,g} \times x_{k,g} \times R_{k,g}}{pop_{1,k,g}}\right) + m_0, \end{aligned} \tag{1}$$

where $pop_{1,k}$ and $pop_{2,k}$ denote the human population and vector population associated with land cover type k, respectively, in areas with overlap between vectors and humans, and w_k is the weight of land cover k. Therefore, $\frac{pop_{2,k}}{pop_{1,k}}$ denotes the average vector density in areas with land cover type k, and $\sum_{k=1}^{l} w_k \left(\frac{pop_{2,k}}{pop_{1,k}}\right)$ denotes the average vector density at the entire location

(e.g., the district) with l types of land cover. G_{total} denotes the number of grids with all land cover types at this location, and G^k_{total} denotes the number of grids of with the land cover type k at this location. Based on the assumed linear relationship between the vector population and rainfall R, the vector population in grid g with land cover type k, denoted as $pop_{2,k,g}$, is calculated as $pop_{2,k,g} = o_{2,k,g} \times x_{k,g} \times R_{k,g}$, where $o_{2,k,g}$ is the vector occurrence probability in grid g with land cover type k, $R_{k,g}$ is the rainfall amount in grid g with land cover type k (unit is mm), and $x_{k,g}$ represents the number of mosquitoes brought by per mm of rainfall in grid g with land cover type k. The variable $pop_{1,k,g}$ denotes the number of humans in grid g with land cover type k, and m_0 is the intercept in the regression model, which can be interpreted as the baseline mosquito density at a given location.

2.3. Modeling malaria transmission via spatiotemporal network

Malaria transmission is caused by the interaction among three key components: a vector, a human, and a parasite. These components are the basic interacting components associated with vector-borne infectious diseases (Xia et al., 2017). The process of malaria transmission between humans and mosquitoes can be depicted by a set of differential equations (DEs) with biological and behavioral parameters that are influenced by complex environmental factors. In this study, we use a host-vector susceptible-latent-infected-susceptible (SLIS) model (Xiao & Zou, 2013) to describe the local malaria transmission, which takes into account the latent period of vectors in addition to the susceptibility and infection state of humans and vectors. The model details can be found in the Supplementary Material.

In addition to the transmission driven by the local environment at individual locations, human mobility among different locations is a key factor that leads to the persistence of malaria epidemics (Cosner et al., 2009; Prosper et al., 2012) and the spread of drug-resistant parasites (Guyant et al., 2015). Such a cross-location human mobility pattern can be described as a general population mobility matrix S:

$$\begin{pmatrix} -\sum_{j=1,j\neq i}^{N}\pi_{j,1} & \pi_{1,2} & \cdots & \pi_{1,N} \\ \pi_{2,1} & -\sum_{j=1,j\neq i}^{N}\pi_{j,2} & \cdots & \pi_{2,N} \\ \vdots & \vdots & \ddots & \vdots \\ \pi_{N,1} & \pi_{N,2} & \cdots & -\sum_{j=1,j\neq i}^{N}\pi_{j,N} \end{pmatrix}, \tag{2}$$

where $\pi_{i,j}$ $(i \neq j)$ is the element in the i th row and the j th column of matrix S, denoting the proportion of the population at the j th location that moves to the i th location per time unit (the unit to be used is based on the temporal scale in the specific model). To parameterize the human mobility matrix, we construct it based on a radiation model (Simini et al., 2012) with both spatial and temporal components. The spatial component is directly calculated by the economic data and the temporal component is inferred from available empirical observations. More details can be found in the Supplementary Material.

By combining the local transmission described by the SLIS model and the cross-location mobility described by Eq. (2), we can formulate an integrative ordinary differential equation system to comprehensively characterize the heterogeneous transmission process at and between locations at the metapopulation level:

$$\begin{cases} \dfrac{dI_{1,i}(t)}{dt} = a_i e_{1,i} m_i S_{1,i} \dfrac{I_{2,i}(t)}{Pop_{2,i}} - r_{1,i} I_{1,i}(t) + \sum_{j=1,j\neq i}^{N} \pi_{i,j} I_{1,j}(t) - \sum_{j=1,j\neq i}^{N} \pi_{j,i} I_{1,i}(t) \\ \dfrac{dL_{2,i}(t)}{dt} = a_i e_{2,i} S_{2,i} \dfrac{I_{1,i}(t)}{Pop_{1,i}} - (\varepsilon_{2,i} + d_{2,i}) L_{2,i}(t) \qquad , i = 1, \ldots, N, \\ \dfrac{dI_{2,i}(t)}{dt} = \varepsilon_{2,i} L_{2,i}(t) - d_{2,i} I_{2,i}(t) \end{cases} \tag{3}$$

where $I_{1,i}$, $L_{2,i}$ and $I_{2,i}$ denote the number of infected human individuals, the number of latent vectors, and the number of infected vectors at location i, respectively; $Pop_{1,i}$ and $Pop_{2,i}$ are the population of humans and that of vectors at location i respectively; and $S_{1,i} = (Pop_{1,i} - I_{1,i}(t))$ and $S_{2,i} = (Pop_{2,i} - L_{2,i}(t) - I_{2,i}(t))$ are the number of susceptible humans and that of vectors respectively. Detailed explanations of all parameters and variables used in Eq. (3) and the rest of the paper are provided in Table 1.

Table 1
Notations and descriptions.

Notation	Description	Values (Calculated from)	Attribute
I_1	The size of the infectious human population	Historical malaria data	Time varying
I_2	The size of the infectious vector population	N.A.[a]	N.A.
L_2	The size of the latent vector population	N.A.	N.A.
a	The daily biting rate of an individual female mosquito on humans	Temperature (Fan & van den Dool, 2008)	Time varying
m	The number of female mosquitoes per person (vector density)	N.A.	N.A.
m_0	The intercept in the formula of vector density	To be estimated	Time invariant
e_1	The fraction of mosquitoes with sporozoites that actually generate infection (and infectiousness) when biting an uninfected person (transmission efficiency from mosquitoes to humans)	N.A.	N.A.
e_2	The proportion of bites by which one susceptible mosquito becomes infected (transmission efficiency from humans to mosquitoes)	N.A.	N.A.
β	The transmission efficiency between humans and mosquitoes ($e_1 \times e_2$)	To be estimated	Time invariant
b_1	The natural birth rate of humans	0	Time invariant
b_2	The natural birth rate of female mosquitoes	N.A.	N.A.
d_1	The natural death rate of humans	0	Time invariant
d_2	The natural death rate of female mosquitoes	Temperature (Fan & van den Dool, 2008)	Time varying
r_1	The average daily recovery rate of an infectious human individual	To be estimated	Time invariant
${\varepsilon_2}^{-1}$	The mean exposure time (remaining in the latent classes) of female mosquitoes	Temperature (Fan & van den Dool, 2008)	Time varying
w_k	The weight of land cover k	land cover (Friedl & Sulla-Menashe, 2015)	Time invariant
G_{total}	The number of grids with all land cover types at this location	land cover (Friedl & Sulla-Menashe, 2015)	Time invariant
G^k_{total}	The number of grids with the land cover type k at this location	land cover (Friedl & Sulla-Menashe, 2015)	Time invariant
$x_{k,g}$	The number of mosquitoes brought by per mm of rainfall in grid g with land cover type k	To be estimated	Time invariant
$o_{2,k,g}$	The occurrence probability of a vector in grid g with land cover type k	Vector distribution (Moyes et al., 2016) and land cover (Friedl & Sulla-Menashe, 2015)	Time invariant
$pop_{1,k,g}$	Human population in grid g with land cover type k	Human population density (Facebook Connectivity Lab and Center for International Earth Science Information Network, 2016) and land cover (Friedl & Sulla-Menashe, 2015)	Time invariant
$R_{k,g}$	The rainfall in grid g with land cover type k	Rainfall (Schneider et al., 2011) and land cover (Friedl & Sulla-Menashe, 2015)	Time varying
F	The matrix representing the temporal patterns of human mobility	To be estimated	Time varying
Q	The matrix representing the spatial patterns of human mobility	Socioeconomic indicators	Time invariant

[a] Not applicable.

2.4. Modeling local and cross-location malaria transmission intensities via the next-generation matrix

According to the SLIS model for single locations (without considering the human mobility for cross-location transmission), the local malaria transmission intensity can be formulated as follows:

$$R_{mo,i} = \frac{a_i^2 e_{1,i} e_{2,i} m_i \varepsilon_{2,i}}{r_{1,i} d_{2,i} (\varepsilon_{2,i} + d_{2,i})}. \tag{4}$$

Here the local transmission intensity $R_{mo,i}$ represents the number of secondary infections of human brought by a single human malaria case in a region i during the month mo, which is consistent with the concept of the basic reproduction number (Diekmann et al., 1990; Van Den Driessche & Watmough, 2002).

After taking human mobility into consideration, we expand the formulation of transmission intensity from the single-location scenario to the multi-location scenario. Based on Eq. (3), we can construct the next-generation matrix (NGM) (Cosner et al., 2009; Diekmann et al., 2010) of the malaria transmission as follows:

$$\mathbf{K}_t = \begin{pmatrix} \mathbf{0} & AE_1M\boldsymbol{\varepsilon}_2(D_2(D_2+\boldsymbol{\varepsilon}_2))^{-1} \\ AE_2\left(-(S-R_1)^{-1}\right) & \mathbf{0} \end{pmatrix}, \tag{5}$$

where A, E_1, E_2, D_2, R_1, M, and $\boldsymbol{\varepsilon}_2$ are $N \times N$ diagonal matrices with diagonal elements a_i,$e_{1,i}$,$e_{2,i}$,$d_{2,i}$,$r_{1,i}$,m_i,and $\varepsilon_{2,i}$ $(i = 1, 2, \ldots, N)$, respectively, and S is the human mobility matrix. Then we can define the malaria transmission matrix P of multiple locations:

$$\begin{aligned} \boldsymbol{I}_1^{t+1} &= P\boldsymbol{I}_1^t, \\ P &= \left(AM\boldsymbol{\varepsilon}_2(D_2(D_2+\boldsymbol{\varepsilon}_2))^{-1}AE_1E_2\right)\left(-(S-R_1)^{-1}\right). \end{aligned} \tag{6}$$

Accordingly, the malaria transmission intensity at location i during a specific month mo can be represented as the sum of all the elements in the i th row of matrix P:

$$R_{mo,i}^{multiple} = \sum_{j=1}^{N} P_{ij}. \tag{7}$$

For the situation of considering multiple locations, based on our definition of malaria transmission matrix P, the $R_{mo,i}^{multiple} = \sum_{j=1}^{N} P_{ij}$ can be interpreted as the number of secondary infections in region i if there exists one human malaria case in each of the N regions. To provide clear and specific guidance for malaria control, we decompose the parameters associated with transmission intensity into two categories: human risk factors, represented by a function f_{human}, and vector risk factors, depicted by a function f_{vector}:

$$f_{vector,i} = \frac{a_i^2 e_{2,i} m_i \varepsilon_{2,i}}{d_{2,i}(\varepsilon_{2,i} + d_{2,i})}, \quad f_{human,i} = \frac{R_{mo,i}^{multiple}}{f_{vector,i}}, \tag{8}$$

where $f_{vector,i}$ represents the generalized formulation of VCAP that considers temperature, rainfall, vector distributions, and land cover types, while $f_{human,i}$ is a non-linear function that takes into account the human mobility, the human recovery rate, and the transmission efficiency from vectors to humans.

Based on the malaria transmission matrix P, we define the imported and exported malaria transmission intensity at location i as follows:

$$\begin{aligned} R_{i,imported}^{multiple} &= \sum_{j=1, j\neq i}^{N} P_{ij}, \\ R_{i,exported}^{multiple} &= \sum_{j=1, j\neq i}^{N} P_{ji}. \end{aligned} \tag{9}$$

2.5. Multivariate regression model for risk prediction

Based on the definition of malaria transmission intensity matrix of multiple locations introduced in Eq. (6), we can formulate a multivariate regression model with nonlinear parameters and noise terms to predict the future malaria risk based on the ground-truth of malaria risk in previous time step:

$$\begin{cases} I_{1,1}^{t+1} = P_{1,1}I_{1,1}^t + P_{1,2}I_{1,2}^t + \ldots + P_{1,N}I_{1,N}^t + \varepsilon_1^t \\ I_{1,2}^{t+1} = P_{2,1}I_{1,1}^t + P_{2,2}I_{1,2}^t + \ldots + P_{2,N}I_{1,N}^t + \varepsilon_2^t \\ \cdots \\ I_{1,N}^{t+1} = P_{N,1}I_{1,1}^t + P_{N,2}I_{1,2}^t + \ldots + P_{N,N}I_{1,N}^t + \varepsilon_N^t \end{cases}, \tag{10}$$

where $I_{1,i}^t$ is the number of human infections at the i th location at time step t, ε_i^t is the noise term for the i th location at time step t, and $P_{i,j}$ represents the element in the i th row and j th column of matrix P. Let $\boldsymbol{y}^{t+1} = [y_1^{t+1}, y_2^{t+1}, \cdots, y_N^{t+1}]^T$ with $y_i^{t+1} = I_{1,i}^{t+1}$, $\boldsymbol{x}^t = \boldsymbol{I}_1^t = [I_{1,1}^t, I_{1,2}^t, \cdots, I_{1,N}^t]^T$, and $\boldsymbol{\varepsilon}^t = [\varepsilon_1^t, \varepsilon_2^t, \cdots, \varepsilon_N^t]^T$; then we can obtain the following equation for all locations at time step t:

$$\boldsymbol{y}^{t+1} = P\boldsymbol{x}^t + \boldsymbol{\varepsilon}^t. \tag{11}$$

Thus, letting $\boldsymbol{Y} = [\boldsymbol{y}^2, \boldsymbol{y}^3, \cdots, \boldsymbol{y}^T]$, $\boldsymbol{X} = [\boldsymbol{x}^1, \boldsymbol{x}^2, \cdots, \boldsymbol{x}^{T-1}]$, and $\boldsymbol{\varepsilon} = [\boldsymbol{\varepsilon}^1, \boldsymbol{\varepsilon}^2, \cdots, \boldsymbol{\varepsilon}^{T-1}]$, for all time steps, we have:

$$\boldsymbol{Y} = P\boldsymbol{X} + \boldsymbol{\varepsilon} = \boldsymbol{Y}^* + \boldsymbol{\varepsilon}, \tag{12}$$

where $\boldsymbol{Y}$ is the ground truth of the transmission risk (e.g., quantified by the number of infected cases) and $\boldsymbol{Y}^* = P\boldsymbol{X}$ is the predicted values of our model. According to Eq. (12), we obtain the objective function for parameter inference and future risk prediction based on the least squares method, which aims to minimize the noise term (i.e., the difference between predicted values $\boldsymbol{Y}^*$ and the ground-truth $\boldsymbol{Y}$):

$$\min_P \|\boldsymbol{\varepsilon}\|_2^2 = \min_P \|\boldsymbol{Y} - \boldsymbol{Y}^*\|_2^2 = \min_P \|\boldsymbol{Y} - P\boldsymbol{X}\|_2^2. \tag{13}$$

In matrix P, some parameters are directly calculated using the climate data based on domain knowledge (Ceccato et al., 2012; Shi et al., 2020), while the rest are inferred via the standard gradient descent method in optimization. The details of optimization procedure can be found in the Supplementary Material.

3. Results

In this section, we validated the effectiveness of the proposed model by investigating the spatiotemporal malaria transmission patterns and the possible intervention responses in 15 malaria-severe districts in Cambodia from January 2018 to March 2021. First, we presented and analyzed the trajectories of the model-inferred malaria transmission intensity over time in terms of human and vector factors. Then, we mapped the local and cross-district transmission risks to facilitate the intuitive analysis of the characteristics of the malaria transmission risk distribution. Finally, we conducted a sensitivity analysis of the intensity with respect to different factor-related parameters to uncover the quantitative relationships between the influential factors and the transmission intensity, and explored the potential intervention strategies for containing malaria transmission in these districts. For the above-mentioned analysis, we demonstrate and discuss the results of 2018 in this paper in detail and put the results of 2019–2021 (which are in the similar format as the results of 2018) in the Supplementary Material for further reference.

3.1. Inferred malaria transmission intensity in terms of human and vector factors

The distribution of the model-inferred transmission intensity in terms of f_{human} and f_{vector} (refer to Eq. (8)) and temporal trajectories of the intensity in six selected districts in 2018 are shown in Fig. 1. The patterns of temporal intensity variations in different districts were quite different. Based on this, the districts were stratified into three categories: (1) those with an intensity < 1 all of the time; (2) those with an intensity near 1; and (3) those with an intensity > 1 most of the time. We also show the distributions of f_{vector} and f_{human} in both the dry and rainy seasons in the subfigures at the bottom left and top right of Fig. 1.

For f_{vector}, we observed that the values in the rainy season were larger than those in the dry season and they varied across districts. Some districts, such as Chbar Mon, displayed relatively large f_{vector} values, with the corresponding malaria transmission intensity exceeding 1 for most of the year. Other districts, such as Bar Kaev and Pursat, exhibited small f_{vector} values, with the transmission intensity always remaining < 1. In other districts, such as Krakor, Phnum Kravanh, and Stueng Traeng, fluctuations in f_{vector} values reflected instability in the corresponding transmission intensity. These values were varying all around 1. Unlike the f_{vector} values, which reflected obvious heterogeneity across spatial and temporal dimensions, f_{human} values were relatively stable and ranged from 0.2 to 0.35 (mean value over time for each district). However, f_{human} still displayed some temporal heterogeneity in districts such as Stueng Traeng, where the f_{human} value was slightly larger in the rainy season than in the dry season, and Bar Kaev, where the f_{human} value was slightly smaller in the rainy season than in the dry season. These relationships between transmission intensity and the two categories of risk-related factors, f_{vector} and f_{human}, may facilitate the implementation of intervention strategies, such as intensive vector control measures and strengthened mobile population surveillance within targeted time periods and at specific locations for the effective control of malaria transmission.

3.2. Spatiotemporal variations in local malaria transmission intensity

An important aspect of malaria control is evaluating the local malaria transmission intensity to gain insights into the transmission potential based on local transmission conditions. The local transmission intensity was calculated using Eq. (4), which does not take the effect of human mobility into account. The average local intensity for each of the 15 districts and the gridded map for each district are illustrated in Fig. 2. Specifically, Fig. 2(a) and (b) show the intensity maps for all 15 districts for two time periods: April 2018 (end of the dry season) and October 2018 (end of the rainy season). We observed clear spatial and temporal heterogeneity in the transmission intensity. For example, the transmission intensities in Bar Kaev, Stueng

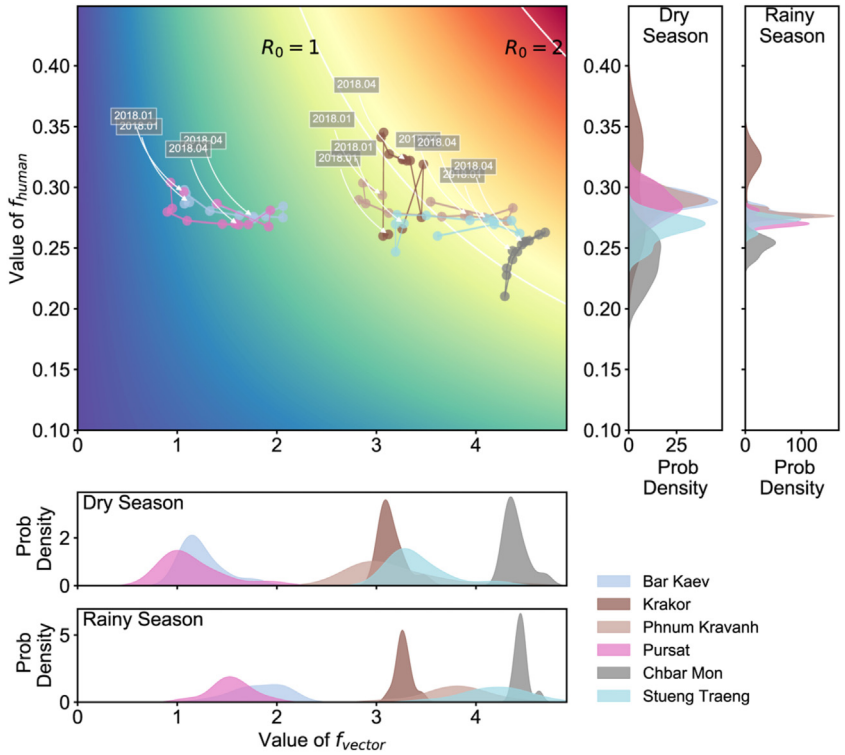

Fig. 1. Inferred malaria transmission intensity in terms of f_{human} and f_{vector} in six malaria-endemic districts in Cambodia from January 2018 to December 2018. The trajectories of the malaria transmission intensity in terms of f_{vector} and f_{human} are shown in the **top left**. The background color illustrates the strength of malaria transmission intensity in ascending order from blue to red; the white lines show the thresholds of $R_0 = 1$ and $R_0 = 2$. In the **bottom left**, the distributions of f_{vector} in different districts during the dry (from November to April) and rainy (from May to October) seasons, calculated using kernel density estimation, are shown. In the **top right,** the distributions of f_{human} in different districts during the dry and rainy seasons are shown.

Traeng, and Phnum Kravanh in April 2018 diverged greatly from those in October 2018. Moreover, the intensities in these three districts within the same period were highly variable, indicating spatial heterogeneity.

Importantly, even though some districts exhibited similar average intensities, the patterns of intrinsic transmission intensity were quite heterogeneous. Fig. 2(c) shows detailed gridded maps of the transmission intensity in all 15 districts in October 2018. Here, Phnum Kravanh and Odongk are used as examples. Both districts had similar average intensities (1.19 for Phnum Kravanh and 1.21 for Stueng Traeng in October 2018). However, the gridwise intensity maps show clear differences in the fine-scale intensity results for each district. In Phnum Kravanh (the first map in the third row of Fig. 2(c), malaria transmission risk was mainly concentrated in the north; in Stueng Traeng (the third map in the fourth row of Fig. 2(c), transmission risk was mainly concentrated in the middle and south. The discovery of such fine-scale heterogeneity is important for guiding location-specific intervention measures, as even for districts with similar average intensities, different public health responses may be required to effectively allocate resources to locations with the greatest need (e.g., villages with the highest transmission risk).

The isolines shown in the maps in Fig. 2(c) indicate the human population density. Interestingly, the areas or grids with the highest population densities were not necessarily those with the highest transmission risk. This may be because the vector density in these areas with high population densities was relatively low. For example, in Saen Monourom, Stueng Traeng, and Phnum Kravanh, the grids with relatively high transmission intensities were generally located in sparsely populated areas. Such areas are also usually remote, comprising the edges of forests and fields. This information is practically useful for implementing tailor-made intervention strategies, such as strengthening the active surveillance of populations in the planting and harvest seasons, especially in hard-to-reach areas.

3.3. Spatiotemporal variations in cross-location malaria transmission intensity

Given the continuous reduction in the number of indigenous cases in recent years, imported malaria has played an increasingly important role in the persistence and resurgence of transmission. Based on the inferred malaria transmission intensity matrix, we easily visualized the spatiotemporal patterns in cross-location transmission intensity. We precisely identified areas with the highest imported and exported risks based on the visualization results, which may prove crucial for determining the best intervention measures in a timely and accurate manner.

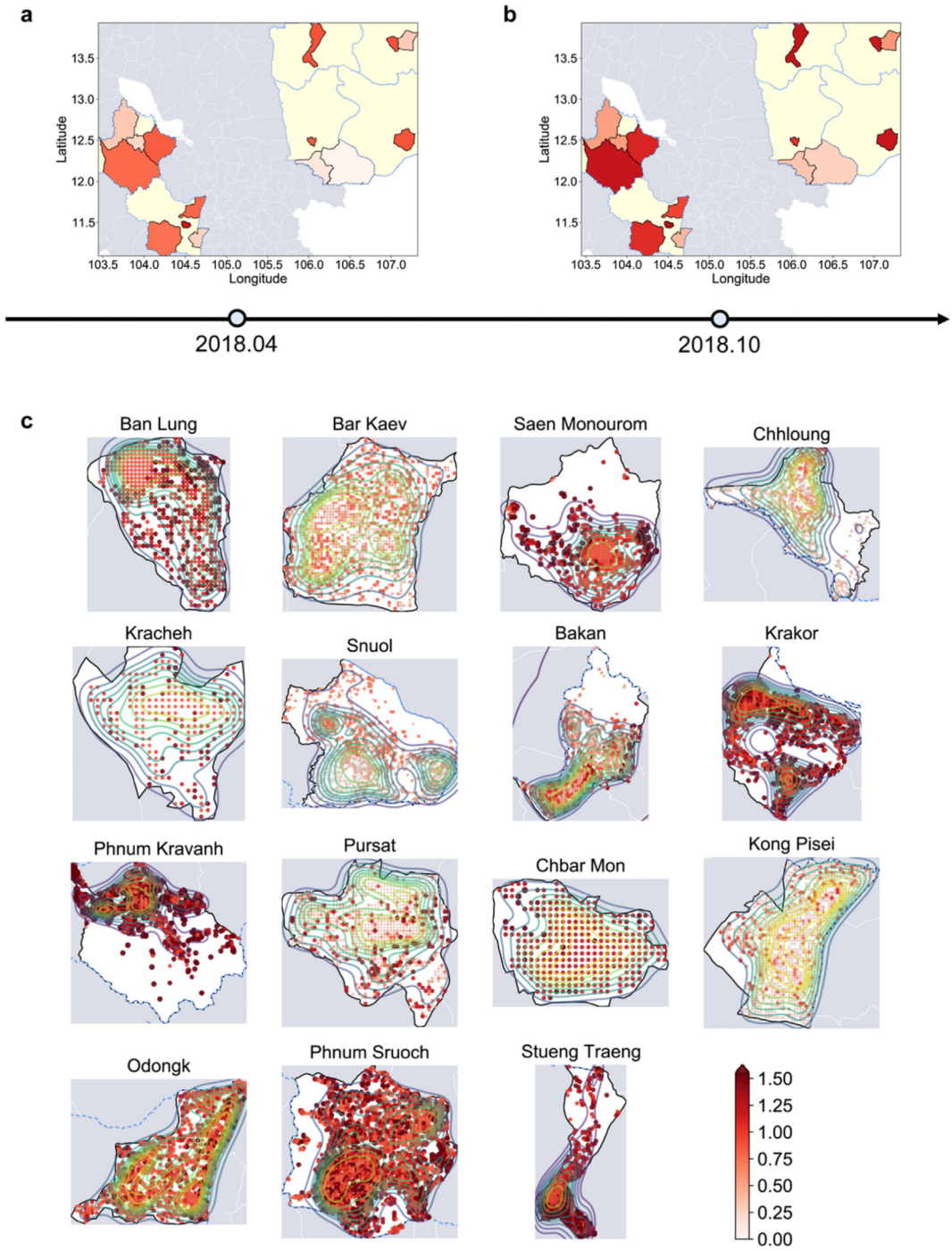

Fig. 2. Spatiotemporally varying maps of the local malaria transmission intensity in all 15 malaria-endemic districts in Cambodia. (a) The average local malaria transmission intensity map for April 2018 (end of the dry season). **(b)** The average local malaria transmission intensity map for October 2018 (end of the rainy season). The color indicates the intensity of malaria transmission, with a darker color indicating higher intensity. **(c)** Gridwise map of the local malaria transmission intensity for each district in October 2018. For the malaria transmission intensity in panels **a**, **b**, and **c**, please refer to the color bar at the bottom of this figure. In panels **a** and **b**, the light yellow background and light blue line in the map show the province boundaries and the gray background and white line denote districts not included in this study. In panel **c**, the grids in the map (with a grid resolution of 500 m $\times$ 500 m) denote the malaria transmission intensity at different locations, and the size and color of each point indicate the corresponding strength of the transmission intensity; the isolines in the maps indicate the human population density at the corresponding locations; the yellow isolines indicate high population density and the dark purple ones indicate low population density; the white background and black line denote the district boundaries.

From the maps in the third and fourth rows in Fig. 3, we further identified several districts with high imported and exported transmission intensities. The patterns of imported intensities (third row in Fig. 3) showed that D3 (Saen Monourom), D8 (Krakor), and D11 (Chbar Mon) displayed high importation levels (indicating higher imported risks) than other districts at the end of the dry season; D9 (Phnum Kravanh), D11 (Chbar Mon), and D3 (Saen Monourom) displayed high importation levels at the end of the rainy season. The patterns of exported intensities (fourth row in Fig. 3) showed that D1 (Ban Lung), D11 (Chbar Mon), and D13 (Odongk) exhibited higher exportation levels (indicating higher exported risks) than other districts at the end of the dry season and D7 (Bakan), D11 (Chbar Mon), and D13 (Odongk) displayed higher exported intensities than other districts at the end of the rainy season. These observations may help further guide mobility restriction policies for areas with relatively high intensities or risks to effectively control disease transmission. The detailed rankings of the imported and exported intensities for these 15 districts are shown in the bar chart in the first row of Fig. 3.

3.4. Factor-risk relationship discovery via sensitivity analysis

In addition to inferring and investigating malaria transmission patterns, we conducted a sensitivity analysis of model parameters to examine the influence of parameter variations for providing insights into the effectiveness of control interventions in different situations. We used the maximum eigenvalue of the transmission intensity matrix to represent the overall malaria transmission intensity in all 15 districts in Cambodia, i.e., $R_{all} = \rho(P)$, and increased or decreased the parameters related to vector and human factors by 0% (i.e., keeping the original values), 5%, 10%, 15%, 20%, and 25% in all districts. The variations in the overall transmission intensity with respect to the variations in the four representative parameters, a, d_2, m, and r_1, are shown in Fig. 4, and that with respect to the variations in other parameters is provided in the Supplementary Figs. S18 and S19.

Specifically, the baseline values of the model parameters (i.e., the values without any change) were calculated in different ways as described in the Supplementary Material. Some parameters, such as the human biting rate a, the latent period of the parasite in mosquitoes ${\varepsilon_2}^{-1}$, and the natural death rate of mosquitoes d_2, can be estimated from the environmental data (i.e., temperature data) based on the empirical knowledge. Since the temporal and spatial resolutions of the temperature are monthly and district-wise, respectively, the values of these data vary over time and space. An example of the value of the temperature and that of these three parameters from 2018.02 to 2021.03 in the district Ban Lung can be found in Supplementary Fig. S1. Other parameters, such as the transmission efficiency from humans to mosquitoes e_2, the transmission efficiency from mosquitoes to humans e_1, and the human recovery rate r_1, can be inferred from data by our method. To infer the values of these parameters, we assigned an initial value to each of them, and used our algorithm iteratively update the values based on the optimization equations, which are shown in the Supplementary Material, to fit the data. The transmission efficiency from humans to mosquitoes e_2, the transmission efficiency from mosquitoes to humans e_1, and the human recovery rate r_1, are assumed to be time-invariant and are the same for all locations; these three learned parameters, e_2, e_1, and r_1, are around 0.17, 0.17, and 0.61, respectively. For the vector density m, it was calculated based on Eq. (1) in Section 2.2. This equation considers the time-varying rainfall data, the inferred variables, the distribution of human density, the vector occurrence, and the land cover. Therefore, the vector density also varies over time and space.

As shown in Fig. 4, the impact of parameter variations on the overall transmission intensity R_{all} varies across different parameters. For example, the variations in a and d_2 yielded larger reductions in R_{all} than do changes in other parameters. Additionally, in different periods, the attention and effort needed for disease control and prevention will be different. In general, the malaria transmission intensities in July–September are greater than transmission threshold 1, which could lead to the persistence of malaria in all 15 districts. Therefore, some actions need to be taken to reduce the intensity below the threshold and prevent further disease transmission during this period. For example, in October 2018, if we aim to control R_{all} below 1, we could increase d_2 by approximately 5%, as can be observed in Fig. 4(b), or reduce m by approximately 10%, as can be observed in Fig. 4(c). Here, the increase in d_2 (the natural death rate of mosquitoes) reflects killing the female mosquitoes to decrease the transmission risk, which can be achieved by implementing insecticide-based methods (Brady et al., 2016), such as insecticide-treated nets (ITNs) and indoor residual spraying (IRS). A decrease in m (the vector density) involves reducing the risk of contact between humans and mosquitoes, reducing the birth of mosquitoes, or increasing the death of mosquitoes. Larval source management (Brady et al., 2016), such as regularly applying biological or chemical insecticides to water bodies (World Health Organization, 2013), and insecticide-based methods can be used to control this parameter.

In addition to exploring the impact of parameter control in all districts simultaneously, we further observed the sensitivity of the overall malaria transmission intensity with respect to the parameters of each district individually. To demonstrate the heterogeneity of effects of parameter variation in different districts, we showed the results with respect to the variation of parameter a (human biting rate) in Fig. 5. The results with respect to other parameters can be found in Supplementary Figs. S20–S25, which have similar patterns as that of parameter a. Notably, the variation of the parameters in different districts, at different times, and at different scales will affect the overall transmission intensity to varying degrees. For example, the variation of parameters such as a and d_2 in Chbar Mon will have a large impact on the overall intensity R_{all} in December, and the variation of all parameters in Stueng Traeng may largely affect R_{all} during the rainy season. Such a location/time-specific effect of parameter variation provides valuable information for guiding tailor-made control strategies; e.g., implementing ITNs or IRS in Chbar Mon in December can significantly reduce f_{vector} in the district (as shown in Fig. 1), thus making a direct contribution to controlling the overall malaria transmission intensity in all districts.

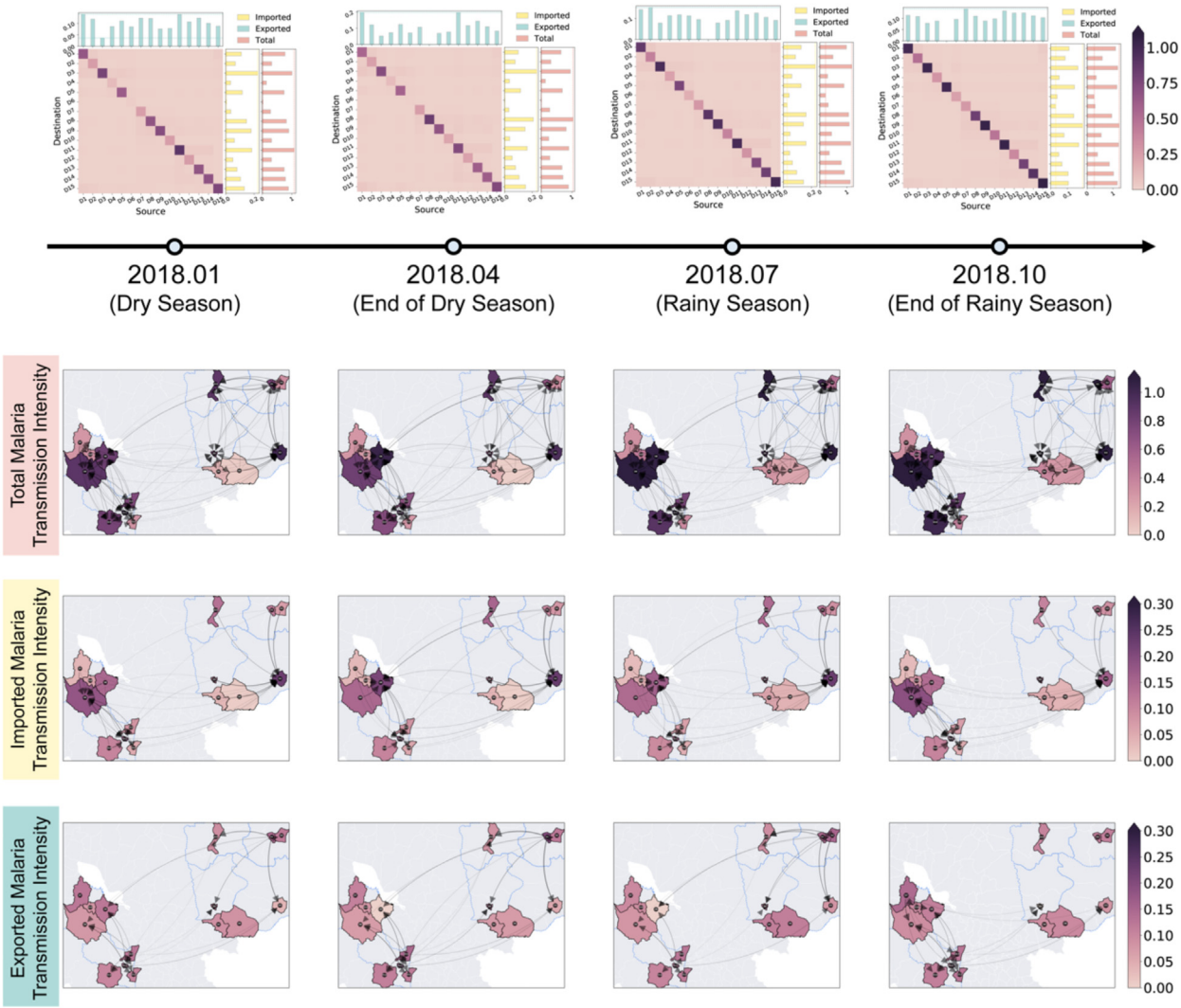

Fig. 3. Spatiotemporal variations in cross-location malaria transmission intensity. The four rows show four types of information: (1) the inferred malaria transmission intensity matrix; (2) the map of total malaria transmission; (3) the map of imported malaria transmission, and (4) the map of exported malaria transmission. The four columns show the results for four different periods in 2018: (1) middle of the dry season (January); (2) end of the dry season (April); (3) middle of the rainy season (July); and (4) end of the rainy season (October). **(First row)** The matrix in the center shows the cross-location malaria transmission intensity. The first bar chart on the right side of the center matrix denotes the intensity or impact of cases of imported malaria from other districts (yellow). The bar chart on the top of the center matrix denotes the intensity or impact of malaria cases exported to other districts (green). The second bar chart on the right side of the center matrix denotes the total malaria intensity calculated after considering the effect of human mobility (pink). The dashed lines in the bar charts denote the bounds of the highest and lowest values. **(Second row)** The color of each district denotes the total malaria transmission intensity; each directed edge denotes the cross-district malaria intensity across different districts. Here, we only show edges with intensities > 0.005. **(Third row)** The color of each district denotes the imported malaria transmission intensity. Here, we only show edges going to districts with the top three imported intensities and those with intensities > 0.005. **(Last row)** The color of each district denotes the exported malaria transmission intensity. Here, we only show edges coming from districts with the top three exported intensities and those with intensities > 0.005. For the value range of the colors, please refer to the color bars on the right side of each row.

4. Discussion

Comprehensively quantifying the malaria transmission intensity by considering heterogeneous risk-related factors and understanding the spatiotemporal transmission patterns are crucial for developing intervention strategies for malaria control and elimination. In this paper, we model the malaria transmission intensity from human, vector, and environmental perspectives and analyze the spatiotemporal patterns of malaria transmission to provide detailed insights regarding endemics and create a valuable reference for planning accurate and timely responses at locations with the greatest needs. In this study, we follow the settings in (Ceccato et al., 2012; Shi et al., 2020) to use a linear model to approximate the relationship between the rainfall and vector density because of the good explainability of the linear model. In fact, the relation between rainfall and

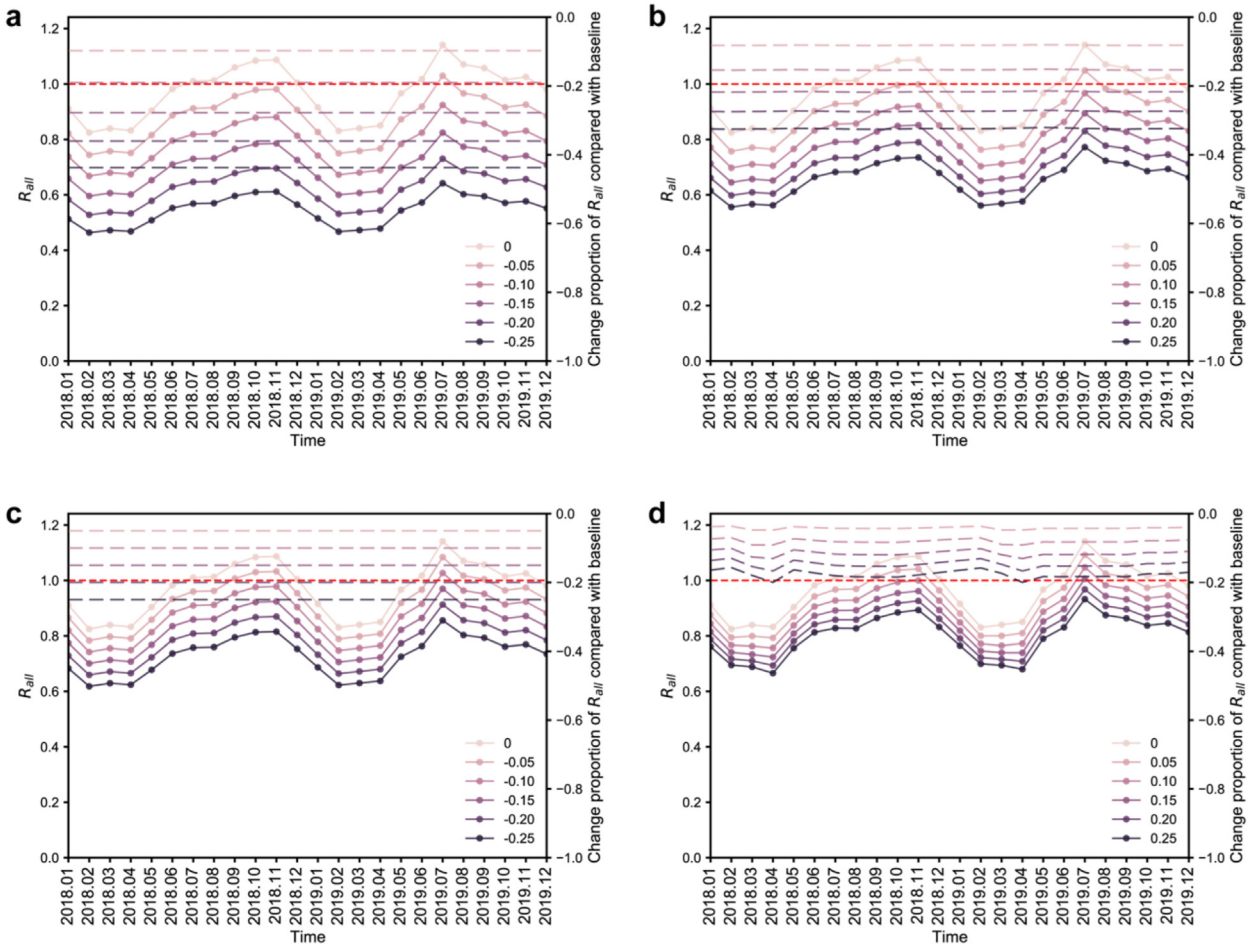

Fig. 4. The sensitivity of the overall malaria transmission intensity with respect to the parameters related to vector factors and human factors. (**a**) a (human biting rate), (**b**) d_2 (mosquito death rate), (**c**) m (vector density), and (**d**) r_1 (human recovery rate). The solid lines denote the value of R_{all} over time with respect to parameter variation. The color intensity of each line indicates the extent of the variation (please see the legend in the subfigures). The darker the color is, the higher the variation percentage. Please refer to the left vertical axis in each subfigure for the detailed values of R_{all}. The dashed lines denote the percentage changes in the value R_{all}. Please refer to the right vertical axis in each subfigure for the detailed values of the changing percentage of R_{all}. The straight red line in each subfigure denotes malaria transmission threshold 1.

vector density could be more complex in reality (Li et al., 2019). Therefore, we plan to explore more sophisticated nonlinear models to represent the relation between them, so as to further enhance the prediction power of the developed model.

It is worth noting that the malaria transmission intensity matrix established with our method is not static but dynamically adaptive over time because it is based on time-varying heterogeneous data and parameters. Our analyses of the inferred transmission intensity patterns in terms of human and vector factors show that 15 pilot districts in Cambodia can be stratified into several groups with different levels of risk, thus enabling us to deploy flexible strategies to control vector and human factors at different locations over time. We map the local malaria transmission intensity at both fine and coarse scales and visualize the cross-location malaria transmission intensity to identify the areas with the highest malaria transmission risk for the accurate implementation of interventions.

Based on the sensitivity analysis of parameters, the proposed model can be used to develop and support various strategies for malaria control and elimination (World Health Organization, 2015, 2017), such as vector control, case detection and management, and malaria surveillance. For vector control, IRS, ITNs, and long-lasting insecticidal nets can reduce the contact between humans and vectors and decrease the mosquito survival, so as to decrease the human biting rate and increase the mosquito death rate. For case control and surveillance, timely tracking and treatment of malaria cases can increase the human recovery rate to curb the further spread of disease.

As pointed out by the Updated Global Technical Strategy for Malaria 2016–2030 (World Health Organization, 2021a), countries that aim to effectively control and eliminate malaria are suggested to adopt tailor-made, data-driven intervention strategies to replace a “one-size-fits-all” method, so as to maximize the utilization of limited anti-malaria resources. Having leapfrogged into malaria elimination, Cambodia's commitment to vanquish the “last mile” of malaria elimination is faced with various obstacles such as artemisinin resistance (Phyo & Nosten, 2018), hard-to-trace human mobility (Guyant et al., 2015),

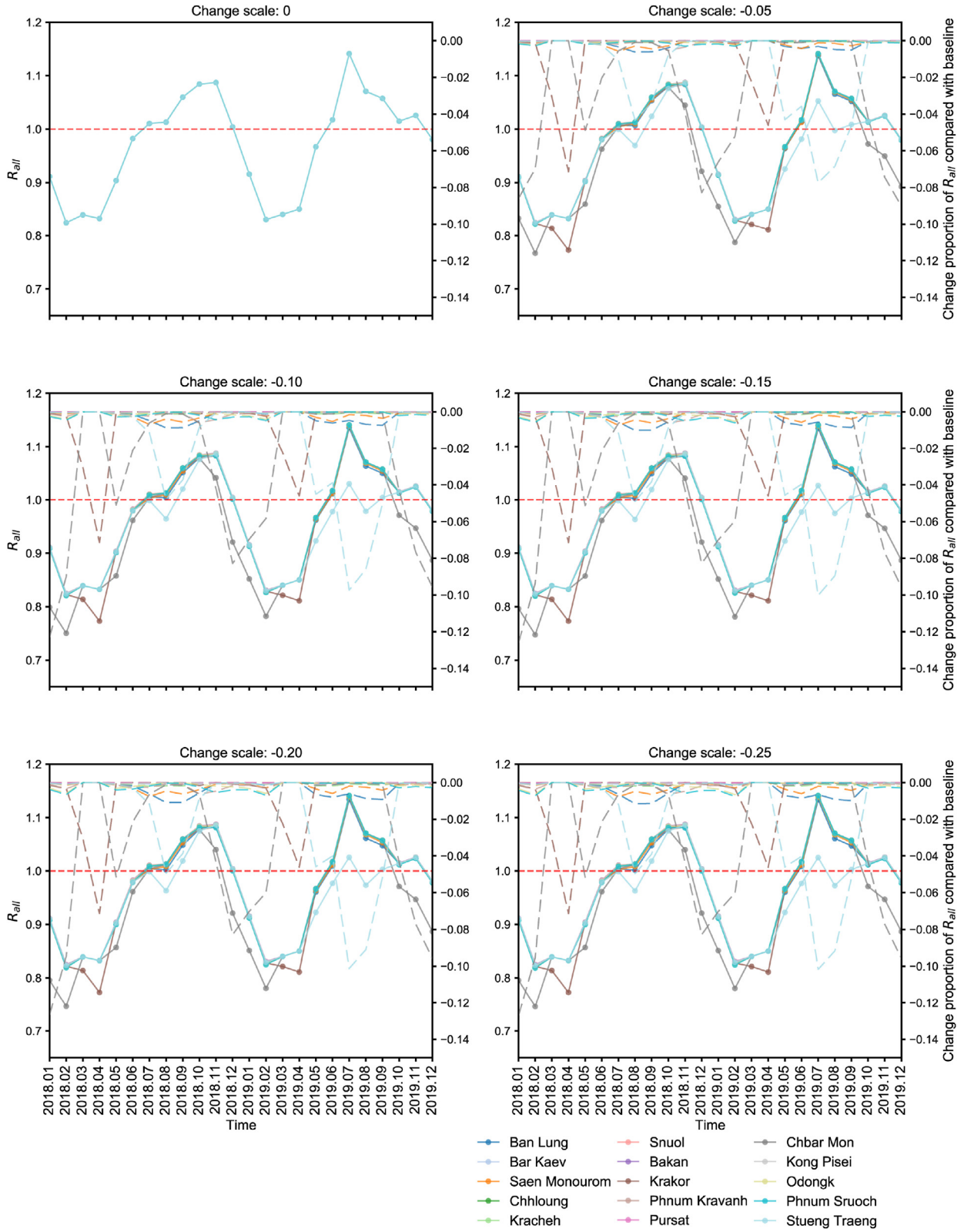

Fig. 5. The sensitivity of the overall malaria transmission intensity with respect to the parameter a **(human biting rate) in individual districts.** In each subfigure, with a fixed percentage change for all districts, as noted in the title of each subfigure, the solid lines denote the R_{all} values over time with respect to the variation of parameter a in different districts (see the legend). Please refer to the left vertical axis in each subfigure for the detailed values of R_{all}. The dashed lines denote the percentage changes in R_{all}. Please refer to the right vertical axis in each subfigure for the detailed values of the changing percentage of R_{all}. The straight red line in each subfigure denotes malaria transmission threshold 1.

and a suitable climate and environment for mosquito breeding (Kar et al., 2014; Kerkhof et al., 2016; Suwonkerd et al., 2013), putting up challenges to public health policy-makers to devise actionable plans that precisely allocate their limited resources to lessen the malaria burden in various regions. Our investigation in Cambodia provides a step-by-step demonstration of the developed integrative risk assessment method in inferring the underlying spatiotemporal malaria transmission intensity from the available empirical observation data and informing corresponding intervention measures. This investigation can also offer evidence-based support and guidance to other malaria-endemic countries and regions that face similar challenges on how targeted intervention strategies can be devised through data-driven approaches to achieve effective malaria control.

The proposed model is a comprehensive and general approach for assessing malaria transmission intensity and is useful for understanding the complex transmission patterns associated with various factors. However, it should be noted that when using the model in other countries or regions, location-specific settings should be considered. For instance, in Africa, the ratio of indigenous cases to imported cases, human social activities, and distributions of land cover and vector species are quite different from those in Cambodia. Consequently, the numerical results reported in this paper may not be directly applicable to other countries or regions, and domain-specific data and information are required to generate context-aware analysis results and guide tailor-made public health responses. Moreover, when implementing intervention strategies for different countries or regions, local conditions such as the cost-effectiveness, availability of health facilities, and operational capacity should be balanced and taken into consideration (Brady et al., 2016).

In addition to the risk-related factors that we have investigated and discussed in this study, other influential factors may also impact the malaria transmission, e.g., the intervention coverage, the immunity level of the population, and the accessibility of healthcare facilities. In fact, the malaria cases in Cambodia in recent years (including the study duration of this work, i.e., from January 2018 to March 2021) obviously demonstrated a decreasing trend, which should be attributed to the effective intervention strategies, e.g., the establishment of village malaria workers (VMWs) for active diagnosis and treatment (Ministry of Health Kingdom of Cambodia, 2021). By fitting the data using a least squares regression, our model implicitly takes such intervention effects into account in a data-driven manner. In our future work, we plan to collect and explicitly incorporate more information about the aforementioned intervention implementations as well as other related data (e.g., the entomological data) to further improve the prediction accuracy and the explainability of the developed model.

Funding

This research was funded by the Ministry of Science and Technology of China (2021ZD0112501/2021ZD0112502), the HKSAR Research Grants Council (12201318/12201619/12202220), and the HKBU/CSD Departmental Start-up Fund for New Assistant Professors.

Author contributions

ML, YL, and JL conceived and designed the research conceptualization, developed the methodology, and drafted the paper. All authors (i.e., ML, YL, SX, LP, RH, XZ, and JL) analyzed the data and revised the paper. All authors approved the final manuscript.

Data availability

The malaria case data are not publicly available because they are nationally owned data. However, they are available from the authors upon reasonable request and with permission of the National Center for Parasitology, Entomology and Malaria Control, Cambodia (CNM). The risk-related data described in Section 2.1 are publicly available at the provided links. The source code used to construct the model and conduct the analyses will be made publicly available once the article is accepted.

Declaration of competing interest

The authors declare that they have no known competing financial interests or personal relationships that could have appeared to influence the work reported in this paper.

Appendix A. Supplementary data

Supplementary data to this article can be found online at https://doi.org/10.1016/j.idm.2023.01.006.

References

Amek, N., Bayoh, N., Hamel, M., Lindblade, K. A., Gimnig, J. E., Odhiambo, F., Laserson, K. F., Slutsker, L., Smith, T., & Vounatsou, P. (2012). Spatial and temporal dynamics of malaria transmission in rural Western Kenya. *Parasites & Vectors, 5*(1), 1–13. https://doi.org/10.1186/1756-3305-5-86

Amoah, B., McCann, R. S., Kabaghe, A. N., Mburu, M., Chipeta, M. G., Moraga, P., Gowelo, S., Tizifa, T., van den Berg, H., Mzilahowa, T., Takken, W., van Vugt, M., Phiri, K. S., Diggle, P. J., Terlouw, D. J., & Giorgi, E. (2021). Identifying Plasmodium falciparum transmission patterns through parasite prevalence and entomological inoculation rate. *Elife, 10*(13050800), 1–32. https://doi.org/10.7554/eLife.65682

Battle, K. E., Lucas, T. C. D., Nguyen, M., Howes, R. E., Nandi, A. K., Twohig, K. A., Pfeffer, D. A., Cameron, E., Rao, P. C., Casey, D., Gibson, H. S., Rozier, J. A., Dalrymple, U., Keddie, S. H., Collins, E. L., Harris, J. R., Guerra, C. A., Thorn, M. P., Bisanzio, D., … Gething, P. W. (2019). Mapping the global endemicity and clinical burden of plasmodium vivax, 2000–17: A spatial and temporal modelling study. *The Lancet, 394*(10195), 332–343. https://doi.org/10.1016/S0140-6736(19)31096-7

Bennett, A., Kazembe, L., Mathanga, D. P., Kinyoki, D., Ali, D., Snow, R. W., & Noor, A. M. (2013). Mapping malaria transmission intensity in Malawi, 2000-2010. *The American Journal of Tropical Medicine and Hygiene, 89*(5), 840–849. https://doi.org/10.4269/ajtmh.13-0028

Brady, O. J., Godfray, H. C. J., Tatem, A. J., Gething, P. W., Cohen, J. M., Ellis McKenzie, F., Alex Perkins, T., Reiner, R. C., Tusting, L. S., Sinka, M. E., Moyes, C. L., Eckhoff, P. A., Scott, T. W., Lindsay, S. W., Hay, S. I., & Smith, D. L. (2016). Vectorial capacity and vector control: Reconsidering sensitivity to parameters for malaria elimination. *Transactions of the Royal Society of Tropical Medicine and Hygiene, 110*(2), 107–117. https://doi.org/10.1093/trstmh/trv113

Cano, J., Berzosa, P. J., Roche, J., Rubio, J. M., Moyano, E., Guerra-Neira, A., Brochero, H., Mico, M., Edú, M., & Benito, A. (2004). Malaria vectors in the Bioko Island (Equatorial Guinea): Estimation of vector dynamics and transmission intensities. *Journal of Medical Entomology, 41*(2), 158–161. https://doi.org/10.1603/0022-2585-41.2.158

Ceccato, P., Vancutsem, C., Klaver, R., Rowland, J., & Connor, S. J. (2012). A vectorial capacity product to monitor changing malaria transmission potential in epidemic regions of Africa. *Journal of Tropical Medicine, 2012*. https://doi.org/10.1155/2012/595948

Chhim, S., Piola, P., Housen, T., Herbreteau, V., & Tol, B. (2021). Malaria in Cambodia: A retrospective analysis of a changing epidemiology 2006–2019. *International Journal of Environmental Research and Public Health, 18*(4), 1–20. https://doi.org/10.3390/ijerph18041960

Chitnis, N., Schpira, A., Smith, D., Hay, S. I., Smith, T., & Steketee, R. (2010). *Mathematical modelling to support malaria control and elimination*.

Cohen, J. M., Le Menach, A., Pothin, E., Eisele, T. P., Gething, P. W., Eckhoff, P. A., Moonen, B., Schapira, A., & Smith, D. L. (2017). Mapping multiple components of malaria risk for improved targeting of elimination interventions. *Malaria Journal, 16*(1), 1–12. https://doi.org/10.1186/s12936-017-2106-3

Connor, S. J. (2002). *The use of environmental information systems (EIS) for malaria control planning in Africa*. University of Liverpool.

Cosner, C., Beier, J. C., Cantrell, R. S., Impoinvil, D., Kapitanski, L., Potts, M. D., Troyo, A., & Ruan, S. (2009). The effects of human movement on the persistence of vector-borne diseases. *Journal of Theoretical Biology, 258*(4), 550–560. https://doi.org/10.1016/j.jtbi.2009.02.016

De Oliveira, E. C., Dos Santos, E. S., Zeilhofer, P., Souza-Santos, R., & Atanaka-Santos, M. (2013). Geographic information systems and logistic regression for high-resolution malaria risk mapping in a rural settlement of the southern Brazilian Amazon. *Malaria Journal, 12*(1), 1–9. https://doi.org/10.1186/1475-2875-12-420

Diekmann, O., Heesterbeek, J. A. P., & Metz, J. A. J. (1990). On the definition and the computation of the basic reproduction ratio R0 in models for infectious diseases in heterogeneous populations. *Journal of Mathematical Biology, 28*(4), 365–382. https://doi.org/10.1007/BF00178324

Diekmann, O., Heesterbeek, J. A. P., & Roberts, M. G. (2010). The construction of next-generation matrices for compartmental epidemic models. *Journal of The Royal Society Interface, 7*(47), 873–885. https://doi.org/10.1098/rsif.2009.0386

Eikenberry, S. E., & Gumel, A. B. (2018). Mathematical modeling of climate change and malaria transmission dynamics: A historical review. *Journal of Mathematical Biology, 77*(4), 857–933. https://doi.org/10.1007/s00285-018-1229-7

Facebook Connectivity Lab and Center for International Earth Science Information Network. (2016). *High resolution settlement layer (HRSL). Source imagery for HRSL© 2016 DigitalGlobe*.

Fan, Y., & van den Dool, H. (2008). A global monthly land surface air temperature analysis for 1948-present. *Journal of Geophysical Research Atmospheres, 113*(1), 1–18. https://doi.org/10.1029/2007JD008470

Filipe, J. A. N., Riley, E. M., Drakeley, C. J., Sutherland, C. J., & Ghani, A. C. (2007). Determination of the processes driving the acquisition of immunity to malaria using a mathematical transmission model. *PLoS Computational Biology, 3*(12), 2569–2579. https://doi.org/10.1371/journal.pcbi.0030255

Friedl, M., & Sulla-Menashe, D. (2015). MCD12Q1 MODIS/Terra+Aqua land cover type yearly L3 global 500m SIN grid. *NASA EOSDIS Land Processes DAAC*. https://doi.org/10.5067/MODIS/MCD12Q1.006

Gao, D., & Ruan, S. (2014). Malaria models with spatial effects. In *Analyzing and modeling spatial and temporal dynamics of infectious diseases* (pp. 3–30).

Gemperli, A., Sogoba, N., Fondjo, E., Mabaso, M., Bagayoko, M., Briët, O. J. T., Anderegg, D., Liebe, J., Smith, T., & Vounatsou, P. (2006). Mapping malaria transmission in west and central Africa. *Tropical Medicine and International Health, 11*(7), 1032–1046. https://doi.org/10.1111/j.1365-3156.2006.01640.x

Gething, P. W., Elyazar, I. R. F., Moyes, C. L., Smith, D. L., Battle, K. E., Guerra, C. A., Patil, A. P., Tatem, A. J., Howes, R. E., Myers, M. F., George, D. B., Horby, P., Wertheim, H. F. L., Price, R. N., Müeller, I., Baird, J. K., & Hay, S. I. (2012). A long neglected world malaria map: Plasmodium vivax endemicity in 2010. *PLoS Neglected Tropical Diseases, 6*(9), Article e1814. https://doi.org/10.1371/journal.pntd.0001814

Grietens, K. P., Gryseels, C., Dierickx, S., Bannister-Tyrrell, M., Trienekens, S., Uk, S., Phoeuk, P., Suon, S., Set, S., Gerrets, R., Hoibak, S., Ribera, J. M., Hausmann-Muela, S., Tho, S., Durnez, L., Sluydts, V., D'Alessandro, U., Coosemans, M., & Erhart, A. (2015). Characterizing types of human mobility to inform differential and targeted malaria elimination strategies in Northeast Cambodia. *Scientific Reports, 5*(November), 1–12. https://doi.org/10.1038/srep16837

Guyant, P., Canavati, S. E., Chea, N., Ly, P., Whittaker, M. A., Roca-Feltrer, A., & Yeung, S. (2015). Malaria and the mobile and migrant population in Cambodia: A population movement framework to inform strategies for malaria control and elimination. *Malaria Journal, 14*(1), 1–15. https://doi.org/10.1186/s12936-015-0773-5

Kamya, M. R., Arinaitwe, E., Wanzira, H., Katureebe, A., Barusya, C., Kigozi, S. P., Kilama, M., Tatem, A. J., Rosenthal, P. J., Drakeley, C., Lindsay, S. W., Staedke, S. G., Smith, D. L., Greenhouse, B., & Dorsey, G. (2015). Malaria transmission, infection, and disease at three sites with varied transmission intensity in Uganda: Implications for malaria control. *The American Journal of Tropical Medicine and Hygiene, 92*(5), 903–912. https://doi.org/10.4269/ajtmh.14-0312

Kargas, N., Qian, C., Sidiropoulos, N. D., Xiao, C., Glass, L. M., & Sun, J. (2021). Stelar: Spatio-Temporal tensor factorization with latent epidemiological regularization. In *35th AAAI conference on artificial intelligence, AAAI 2021, 6A* pp. 4830–4837).

Kar, N. P., Kumar, A., Singh, O. P., Carlton, J. M., & Nanda, N. (2014). A review of malaria transmission dynamics in forest ecosystems. *Parasites & Vectors, 7*(1), 1–12. https://doi.org/10.1186/1756-3305-7-265

Kerkhof, K., Sluydts, V., Heng, S., Kim, S., Pareyn, M., Willen, L., Canier, L., Sovannaroth, S., Ménard, D., Sochantha, T., Coosemans, M., & Durnez, L. (2016). Geographical patterns of malaria transmission based on serological markers for falciparum and vivax malaria in Ratanakiri, Cambodia. *Malaria Journal, 15*(1), 1–15. https://doi.org/10.1186/s12936-016-1558-1

Li, R., Xu, L., Bjørnstad, O. N., Liu, K., Song, T., Chen, A., Xu, B., Liu, Q., & Stenseth, N. C. (2019). Climate-driven variation in mosquito density predicts the spatiotemporal dynamics of dengue. *Proceedings of the National Academy of Sciences of the United States of America, 116*(9), 3624–3629. https://doi.org/10.1073/pnas.1806094116

Macdonald, G. (1957). *The epidemiology and control of malaria*. Oxford university press.

Mandal, S., Sarkar, R., & Sinha, S. (2011). Mathematical models of malaria - a review. *Malaria Journal, 10*, 1–19. https://doi.org/10.1186/1475-2875-10-202

Ministry of Health Kingdom of Cambodia. (2021). *Cambodia malaria elimination action framework 2021-2025*.

Moyes, C. L., Shearer, F. M., Huang, Z., Wiebe, A., Gibson, H. S., Nijman, V., Mohd-Azlan, J., Brodie, J. F., Malaivijitnond, S., Linkie, M., Samejima, H., O'Brien, T. G., Trainor, C. R., Hamada, Y., Giordano, A. J., Kinnaird, M. F., Elyazar, I. R. F., Sinka, M. E., Vythilingam, I., … Hay, S. I. (2016). Predicting the geographical distributions of the macaque hosts and mosquito vectors of Plasmodium knowlesi malaria in forested and non-forested areas. *Parasites & Vectors, 9*(1), 1–12. https://doi.org/10.1186/s13071-016-1527-0

Munga, S., Minakawa, N., Zhou, G., Mushinzimana, E., Barrack, O. O. J., Githeko, A. K., & Yan, G. (2006). Association between land cover and habitat productivity of malaria vectors in western Kenyan highlands. *The American Journal of Tropical Medicine and Hygiene, 74*(1), 69–75. https://doi.org/10.4269/ajtmh.2006.74.69

Munga, S., Yakob, L., Mushinzimana, E., Zhou, G., Ouna, T., Minakawa, N., Githeko, A., & Yan, G. (2009). Land use and land cover changes and spatiotemporal dynamics of anopheline larval habitats during a four-year period in a highland community of Africa. *The American Journal of Tropical Medicine and Hygiene, 81*(6), 1079. https://doi.org/10.4269/ajtmh.2009.09-0156.Land

Mushinzimana, E., Munga, S., Minakawa, N., Li, L., Feng, C., Bian, L., Kitron, U., Schmidt, C., Beck, L., Zhou, G., Githeko, A. K., & Yan, G. (2006). Landscape determinants and remote sensing of anopheline mosquito larval habitats in the western Kenya highlands. *Malaria Journal, 5*(1), 1–11. https://doi.org/10.1186/1475-2875-5-13

Obsomer, V., Dufrene, M., Defourny, P., & Coosemans, M. (2013). Anopheles species associations in southeast Asia: Indicator species and environmental influences. *Parasites & Vectors, 6*(1), 1–14. https://doi.org/10.1186/1756-3305-6-136
Olaniyi, S., & Obabiyi, O. S. (2013). Mathematical model for malaria transmission dynamics in human and mosquito populations with nonlinear forces of infection. *International Journal of Pure and Applied Mathematics, 88*(1), 125–156.
Omumbo, J. A., H, S. I., G, S. J., S, R. W., & R, D. J. (2002). Updating historical maps of malaria transmission intensity in East Africa using remote sensing. *Photogrammetric Engineering & Remote Sensing, 68*(2), 161–166.
Omumbo, J. A., Hay, S. I., Snow, R. W., Tatem, A. J., & Rogers, D. J. (2005). Modelling malaria risk in East Africa at high-spatial resolution. *Tropical Medicine and International Health, 10*(6), 557–566. https://doi.org/10.1111/j.1365-3156.2005.01424.x
Onori, E. (1967). Distribution of plasmodium ovale in the eastern, western and northern regions of Uganda. *Bulletin of the World Health Organization, 37*(4), 665–668.
Pei, H., Yang, B., Liu, J., & Chang, K. C. C. (2022). Active surveillance via group sparse bayesian learning. *IEEE Transactions on Pattern Analysis and Machine Intelligence, 44*(3), 1133–1148. https://doi.org/10.1109/TPAMI.2020.3023092
Pei, H., Yang, B., Liu, J., & Dong, L. (2018). Group sparse bayesian learning for active surveillance on epidemic dynamics. In *Proceedings of the thirty-second AAAI conference on artificial intelligence* (pp. 800–807).
Phyo, A. P., & Nosten, F. (2018). The artemisinin resistance in southeast Asia: An imminent global threat to malaria elimination. In S. Manguin, & V. Dev (Eds.), *Towards malaria elimination - a leap forward*. IntechOpen. https://doi.org/10.5772/intechopen.76519.
Prosper, O., Ruktanonchai, N., & Martcheva, M. (2012). Assessing the role of spatial heterogeneity and human movement in malaria dynamics and control. *Journal of Theoretical Biology, 303*, 1–14. https://doi.org/10.1016/j.jtbi.2012.02.010
Routledge, I., Chevéz, J. E. R., Cucunubá, Z. M., Rodriguez, M. G., Guinovart, C., Gustafson, K. B., Schneider, K., Walker, P. G. T., Ghani, A. C., & Bhatt, S. (2018). Estimating spatiotemporally varying malaria reproduction numbers in a near elimination setting. *Nature Communications, 9*(1), 1–8. https://doi.org/10.1038/s41467-018-04577-y
Ruktanonchai, N. W., Smith, D. L., & De Leenheer, P. (2016). Parasite sources and sinks in a patched Ross–MacDonald malaria model with human and mosquito movement: Implications for control. *Mathematical Biosciences, 279*, 90–101. https://doi.org/10.1016/j.mbs.2016.06.012
Rumisha, S. F., Smith, T., Abdulla, S., Masanja, H., & Vounatsou, P. (2014). Modelling heterogeneity in malaria transmission using large sparse spatio-temporal entomological data. *Global Health Action, 7*(1), Article 22682. https://doi.org/10.3402/gha.v7.22682
Schneider, U., Becker, A., Finger, P., Meyer-Christoffer, A., Rudolf, B., & Ziese, M. (2011). GPCC full data reanalysis version 6.0 at 1.0°: Monthly land-surface precipitation from rain-gauges built on GTS-based and historic data. *Global Precipitation Climatology Centre*. https://doi.org/10.5676/DWD_GPCC/FD_M_V7_100
Shi, B., Lin, S., Tan, Q., Cao, J., Zhou, X., Xia, S., Zhou, X. N., & Liu, J. (2020). Inference and prediction of malaria transmission dynamics using time series data. *Infectious Diseases of Poverty, 9*(4), 84–96. https://doi.org/10.1186/s40249-020-00696-1
Shi, B., Zheng, J., Qiu, H., Yang, G.-J., Xia, S., & Zhou, X.-N. (2017). Risk assessment of malaria transmission at the border area of China and Myanmar. *Infectious Diseases of Poverty, 6*(4), 55–63.
Simini, F., González, M. C., Maritan, A., & Barabási, A. L. (2012). A universal model for mobility and migration patterns. *Nature, 484*(7392), 96–100. https://doi.org/10.1038/nature10856
Smith, D. L., & McKenzie, F. E. (2004). Statics and dynamics of malaria infection in Anopheles mosquitoes. *Malaria Journal, 3*(1), 1–14. https://doi.org/10.1186/1475-2875-3-13
Stefani, A., Dusfour, I., Corrêa, A. P. S. A., Cruz, M. C. B., Dessay, N., Galardo, A. K. R., Galardo, C. D., Girod, R., Gomes, M. S. M., Gurgel, H., Lima, A. C. F., Moreno, E. S., Musset, L., Nacher, M., Soares, A. C. S., Carme, B., & Roux, E. (2013). Land cover, land use and malaria in the amazon: A systematic literature review of studies using remotely sensed data. *Malaria Journal, 12*(1), 1–8. https://doi.org/10.1186/1475-2875-12-192
Suwonkerd, W., Ritthison, W., Ngo, C. T., Tainchum, K., Bangs, M. J., & Chareonviriyaphap, T. (2013). Vector biology and malaria transmission in southeast Asia. In S. Manguin (Ed.), *Anopheles mosquitoes-new insights into malaria vectors*. IntechOpen. https://doi.org/10.5772/56347.
Tan, Q., Liu, Y., & Liu, J. (2021). Demystifying deep learning in predictive spatiotemporal analytics: An information-theoretic framework. *IEEE Transactions on Neural Networks and Learning Systems, 32*(8), 3538–3552. https://doi.org/10.1109/TNNLS.2020.3015215
Tanser, F. C., Sharp, B., & Le Sueur, D. (2003). Potential effect of climate change on malaria transmission in Africa. *Lancet, 362*(9398), 1792–1798. https://doi.org/10.1016/S0140-6736(03)14898-2
Van Den Driessche, P., & Watmough, J. (2002). Reproduction numbers and sub-threshold endemic equilibria for compartmental models of disease transmission. *Mathematical Biosciences, 180*(1–2), 29–48. https://doi.org/10.1016/S0025-5564(02)00108-6
Wang, R., Maddix, D., Faloutsos, C., Wang, Y., & Yu, R. (2021). Bridging physics-based and data-driven modeling for learning dynamical systems. *Proceedings of the 3rd Conference on Learning for Dynamics and Control, 144*, 385–398. http://arxiv.org/abs/2011.10616.
Weiss, D. J., Lucas, T. C. D., Nguyen, M., Nandi, A. K., Bisanzio, D., Battle, K. E., Cameron, E., Twohig, K. A., Pfeffer, D. A., Rozier, J. A., Gibson, H. S., Rao, P. C., Casey, D., Bertozzi-Villa, A., Collins, E. L., Dalrymple, U., Gray, N., Harris, J. R., Howes, R. E., … Gething, P. W. (2019). Mapping the global prevalence, incidence, and mortality of plasmodium falciparum, 2000–17: A spatial and temporal modelling study. *The Lancet, 394*(10195), 322–331. https://doi.org/10.1016/S0140-6736(19)31097-9
World Health Organization. (2013). *Larval source management: A supplementary measure for malaria vector control: An operational manual*. World Health Organization.
World Health Organization. (2015). *Strategy for malaria elimination in the greater mekong subregion: 2015-2030*. World Health Organization.
World Health Organization. (2017). *A framework for malaria elimination*. World Health Organization. http://apps.who.int/iris/bitstream/handle/10665/254761/9789241511988-eng.pdf?sequence=1.
World Health Organization. (2021a). *Global technical Strategy for malaria 2016–2030 (2021 update)*. https://www.who.int/publications/i/item/9789240031357.
World Health Organization. (2021b). *World malaria report 2021*. World Health Organization. https://www.who.int/teams/global-malaria-programme/reports/world-malaria-report-2021.
World Health Organization, & Regional Office for South-East Asia. (2017). *Population mobility and malaria*. World Health Organization. https://apps.who.int/iris/handle/10665/255816.
Wu, Y., Yang, Y., Nishiura, H., & Saitoh, M. (2018). Deep learning for epidemiological predictions. *Proceedings of the Forty-First International ACM SIGIR Conference on Research and Development in Information Retrieval*, 1085–1088.
Xiao, Y., & Zou, X. (2013). On latencies in malaria infections and their impact on the disease dynamics. *Mathematical Biosciences and Engineering, 10*(2), 463–481. https://doi.org/10.3934/mbe.2013.10.463
Xia, S., Zhou, X. N., & Liu, J. (2017). Systems thinking in combating infectious diseases. *Infectious Diseases of Poverty, 6*(5), 57–63.
Yang, H. M. (2000). Malaria transmission model for different levels of acquired immunity and temperature-dependent parameters (vector). *Revista de Saúde Pública, 34*(3), 223–231.
Yang, G. J., Gao, Q., Zhou, S. S., Malone, J. B., McCarroll, J. C., Tanner, M., Vounatsou, P., Bergquist, R., Utzinger, J., & Zhou, X. N. (2010). Mapping and predicting malaria transmission in the People's Republic of China, using integrated biology-driven and statistical models. *Geospatial Health, 5*(1), 11–22. https://doi.org/10.4081/gh.2010.183
Yang, B., Guo, H., Yang, Y., Shi, B., Zhou, X., & Liu, J. (2014). Modeling and mining spatiotemporal patterns of infection risk from heterogeneous data for active surveillance planning. *Proceedings of the Twenty-Eighth AAAI Conference on Artificial Intelligence*, 493–499.
Zhang, Y., Cheung, W. K., & Liu, J. (2015). A unified framework for epidemic prediction based on Poisson regression. *IEEE Transactions on Knowledge and Data Engineering, 27*(11), 2878–2892. https://doi.org/10.1109/TKDE.2015.2436918